NASA Technical Memorandum 81320 USAAVRADCOM TR-81-A-24

(NASA-TM-81320) PREDICTION OF BLADE-VORTEX INTERACTION NOISE FROM MEASURED BLADE PRESSURE (NASA) 22 p HC A02/MF A01 CSCL 01A

N81-33157

Unclas
G3/02 27580

Prediction of Blade-Vortex Interaction Noise From Measured Blade Pressure

Yoshiya Nakamura

September 1981

RECEIVED
NASA STI FACILITY
ACCESS DEPT.

National Aeronautics and Space Administration

United States Army Aviation Research and Development Command

NASA Technical Memorandum 81320

USAAVRADCOM TR-81-A-24

Prediction of Blade-Vortex Interaction Noise From Measured Blade Pressure

Yoshiya Nakamura, Aeromechanics Laboratory
AVRADCOM Research and Technology Laboratories
Ames Research Center, Moffett Field, California

National Aeronautics and
Space Administration

Ames Research Center
Moffett Field, California 94035

United States Army
Aviation Research and
Development Command
St. Louis, Missouri 63166

PREDICTION OF BLADE-VORTEX INTERACTION NOISE FROM MEASURED BLADE PRESSURE

Yoshiya Nakamura*

Aeromechanics Laboratory
U.S. Army Research and Technology Laboratories (AVRADCOM)
Ames Research Center
Moffett Field, Calif. 94035, U.S.A.

ABSTRACT

The impulsive nature of noise due to the interaction of a rotor blade with a tip vortex is studied. The time signature of this noise is calculated theoretically based on the measured blade surface pressure fluctuation of an operational load survey rotor in slow descending flight and is compared with the simultaneous microphone measurement. Particularly, the physical understanding of the characteristic features of a waveform is extensively studied in order to understand the generating mechanism and to identify the important parameters. The interaction trajectory of a tip vortex on an acoustic planform is shown to be a very important parameter for the impulsive shape of the noise. The unsteady nature of the pressure distribution at the very leading edge is also important to the pulse shape. The theoretical model using noncompact linear acoustics predicts the general shape of interaction impulse pretty well except for peak amplitude which requires more continuous pressure information along the span at the leading edge.

1. INTRODUCTION

Helicopter impulsive noise that is sometimes called "blade-slap" is the most annoying sound generated by a helicopter. The waveform of this distinct and intensive sound consists of two distinct signatures: First, a series of positive and negative acoustic pressure spikes due to blade-vortex interactions, and second a large negative acoustic pressure peak due to compressibility as shown in Fig. 1. This compressibility noise, sometimes called high speed impulsive noise, is closely connected to the advancing tip Mach numbers, and radiates strong acoustic energy into the tip-path plane in the forward direction. This compressibility noise is determined not only by the boundary conditions on the rotor blade surface but also on the perturbed flow field around the blade, and therefore is a combination of blade thickness and nonlinear effects. On the other hand, the first type of waveform is caused by the aerodynamic interactions between the tip vortices and a following blade. This type of noise is called blade-vortex interaction noise, and is the subject of this paper.

These interactions occur both on the advancing and retreating sides of a rotor disk as shown in Fig. 2; however, the acoustically important interactions are in the first quadrant of the disk, radiating intensive acoustic energy forward and about 30° below the rotor tip-path plane. These interactions rapidly change the local flow field around the blade, can cause unsteady pressure fluctuations, particularly near the blade leading-edge, and can generate shocks on the

*NRC Research Associate, on leave from Ishikawajima-Harima Heavy Industry Co. Ltd., Tokyo.

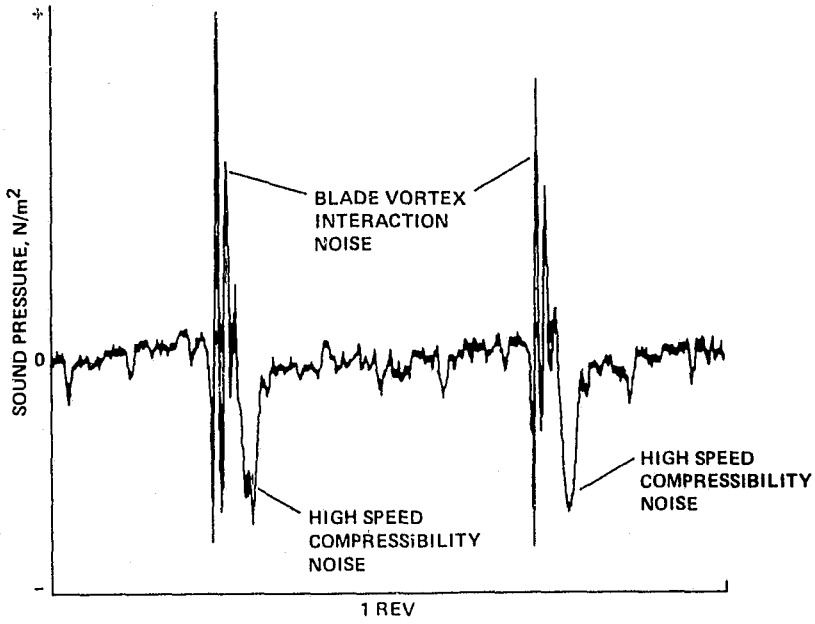


Figure 1. Example of blade slap noise waveform (Ref. 7).

advancing side or stall in the retreating side. The shock on the advancing side is a result of the flow acceleration generated by the vortex below a blade, where stalls on the retreating side are caused by an increased angle of attack induced by the vortex. Among these several mechanisms, the unsteady pressure fluctuation on a blade was identified by several experiments to be the most possible cause of blade-vortex interaction noise in a real environment.

One of the most successful theoretical models for the prediction of blade-vortex interaction noise was developed by Widnall (Ref. 1), who simplified the model as an infinite span blade encountering a straight vortex expressed by a vertical gust. By applying this interaction model to the tip portion of the blade the acoustic pressure signal was obtained with the use of an unsteady lifting-line theory and a linear acoustic theory with a compact source assumption. A good agreement with some model tests was demonstrated. In a recent paper the same model was used, and it was shown that the tip-vortex structure determined by the slope of the spanwise loading distribution, especially at the tip, strongly influences the blade-vortex interaction noise. The simplified vortex model was useful to obtain these findings but unfortunately the blade-vortex interaction noise depends critically on vortex structure, intensity and trajectory. Therefore, this vortex model is not really adequate for the prediction of the actual interaction noise in the real world.

Some qualitative discussions on the relationship of the tip-vortex trajectory and the interaction noise was made by Lowson and Ollerhead (Ref. 3). They argued that the interaction in the first quadrant of the rotor disk is the most

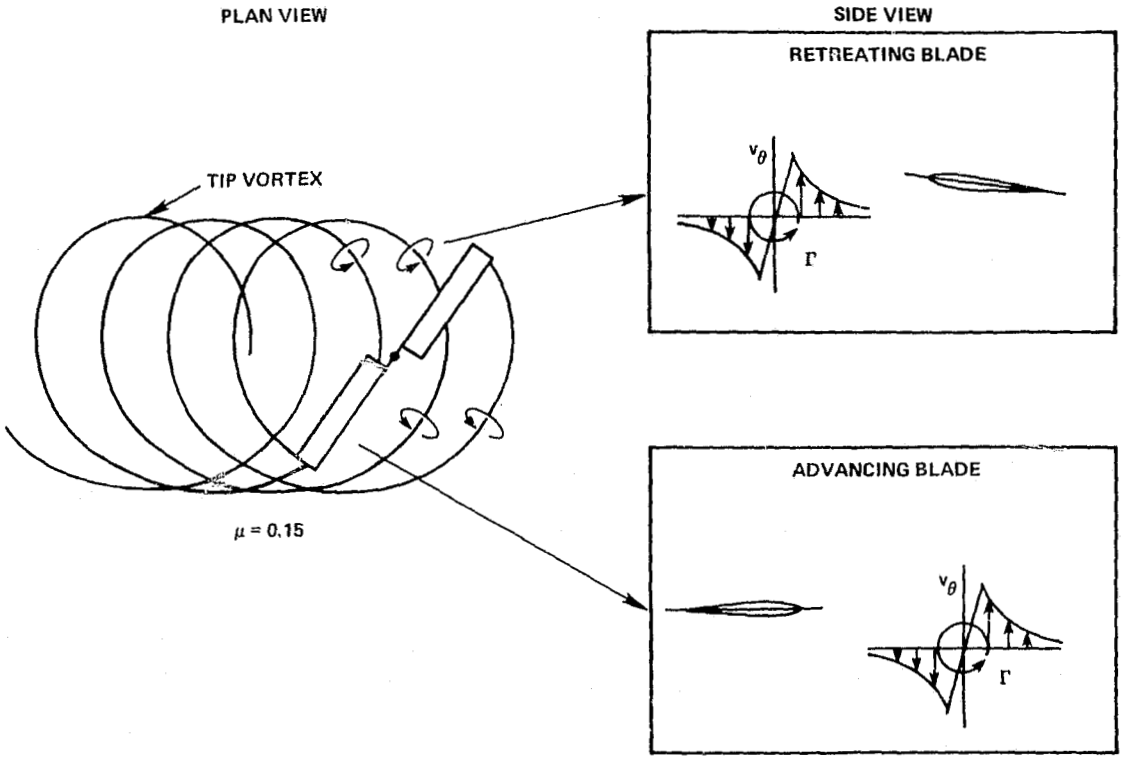


Figure 2. Blade-vortex interactions on advancing side and on retreating side.

important area for the blade-vortex interaction noise especially at high advancing ratio because the angle between the blade span and tip vortex axis is small, and therefore the convection Mach number of the interacting point becomes greater.

In the experimental field, many model rotor tests in hover and in wind tunnels have been conducted to determine the relation of rotor parameters and the associated measured noise level. The full-scale hovering rotor tests just above the ground and whirl towers have also been tried. Some loud impulsive noise was measured but the similarity to the real situation of blade-vortex interaction was left as questionable because of Reynolds or Mach number scaling, wall or ground reflection, or wind shear effects.

In recent years, much more useful information and a better understanding of blade-vortex interaction noise has been obtained through some significant experiments. Tangler (Ref. 4) has shown through the use of Schlieren techniques that the accelerated flow beneath the advancing blade can produce local shock waves. The accelerated flow due to the horizontal velocity component of 1- or 1-1/2-revolution old tip vortices combined with the blade circulation that produced critical velocities. He related the measured acoustic impulse to the shock

propagation. His discovery of possible compressibility effects on the interaction noise was really impressive although the generality of results in the real environment remained uncertain. Another model test by Hoad (Ref. 5) has provided an aerodynamic evaluation of blade-tip shape configuration on noise reduction. He showed that the swept-tapered tip blade was more effective in reducing noise in the far field than the Ogee-tip or the subwing-tip blade. The end-plate-tip blade was more noisy than the reference square-tip blade. Source locations of blade-vortex interaction noise were also estimated by triangulations from measured acoustic data as between 65° to 90° azimuth and 0.6 to 1.0 radii from the hub.

Schmitz and Boxwell (Ref. 6) have successfully obtained high-quality noise data by their unique in-flight far-field measurement technique in the various combinations of airspeeds and rates of descent. They identified two distinct features of pressure signals and corresponding generating mechanisms: a series of positive and negative pressure pulses and a large negative pressure pulse as a blade-vortex interaction effect and a compressibility effect, respectively. And they also argued that both mechanisms have different acoustic directivity patterns: the blade-vortex interaction noise radiates forward and below the rotor plane, whereas the compressibility noise radiates forward in the plane of the rotor disk and strengthens rapidly with advancing tip Mach number. Throughout the more intensive work (Ref. 7) on blade-vortex interaction impulsive noise they found that no definite shocks were formed in descending flight, whereas the very rapid pressure recovery of the in-plane negative pressure pulse definitely could be attributed to a shock-wave pressure recovery. Here, it was shown to be useful to stretch a time history of the pressure impulses to identify shock-wave radiation.

Shockey et al. (Ref. 8) surveyed in-flight aerodynamic, structural, and acoustic data simultaneously in a wide range of operating conditions, and many qualitative relations of noise and aerodynamic events were discussed. These simultaneous measurements of the acoustic field and blade surface-pressure distribution have provided a good opportunity to develop and evaluate a prediction scheme for blade-vortex interaction noise.

In this paper, the impulsive blade-vortex interaction noise is studied. The emphasis has been placed on the prediction of impulsive characteristics of acoustic waveform using the measured blade-surface pressures.

2. EXPERIMENTAL PROCEDURE

A joint U.S. Army/Bell Helicopter Textron flight-test program called the AH-1G Helicopter Operational Load Survey (OLS) was conducted to gain the detailed knowledge of rotor aero- and structural-dynamics including rotor acoustics in forward flight (Refs. 8, 9). The simultaneous measurements of rotor noise and blade surface pressure distribution, particularly the unsteady blade-pressure fluctuations, provided the basis of this study on the impulsive nature of blade-vortex interaction noise. The flight envelope for the acoustic data covered a range of forward speed from 30 knots to 90 knots and descent rates from 0 to 1000 ft/m, and level flight airspeeds up to 165 knots. Among all the combinations of descending flight the case of 65 knots and 200 ft/m descent generated the most intensive blade-vortex interaction noise. Under these conditions the tip vortex may be nearly in the plane of the rotor which would maximize blade-vortex interaction noise. Therefore this case was selected for study in this paper.

Blade Instrumentation

Mounted on the upper and lower airfoil surfaces were 110 Kulite absolute pressure transducers to measure static-pressure distribution. Their spanwise locations were 40, 60, 75, 86.4, and 95.5% radii, and their chordwise locations were 1, 3, 8, 15, 20, 25, 35, 40, 45, 50, 55, 60, 70, and 92% of the chord on both surfaces at each spanwise station as shown in Fig. 3. The pressure signals were recorded by a 28-track tape recorder through rotating FM multiplex systems, slip rings, and static FM multiplex systems. The blade pressure measurement system has a frequency response of 400 Hz; hence, events occurring within approximately 5° of change in rotor azimuth can be measured.

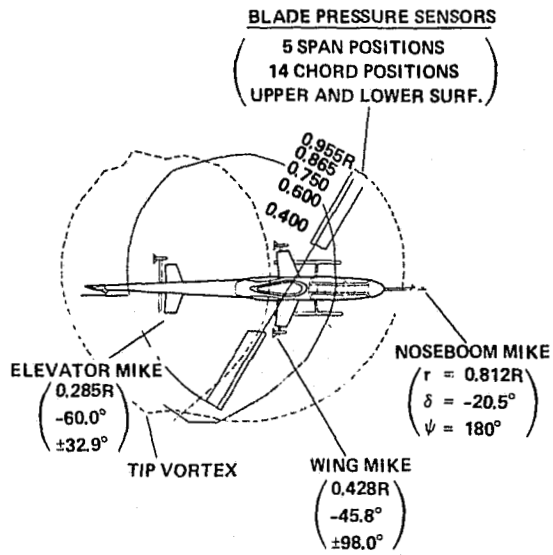


Figure 3. Simultaneous measurement of blade surface pressure and noise.

Acoustic Instrumentation

Five B&K microphones with wind screens were mounted on the aircraft in a symmetrical pattern as shown in Fig. 3. They were located on the nose boom, on the left and right wings, and aft on the ends of the elevator. The signals were conditioned by a multichannel audio amplifier and then recorded on the on-board FM tape recorder at a tape speed of 30 in./sec. This setup provided a frequency response of DC to 10 KHz with a signal to noise ratio of 46 dB rms.

Three ground based microphones were located 500 ft apart on a line perpendicular to the flightpath. But their data were not used in this study.

Complete details for the experimental procedures and instrumentation are given in Refs. 8 and 9.

3. DEVELOPMENT OF PREDICTION METHOD

Basic Equation

As stated in the introduction the unsteady blade-surface-pressure fluctuations seem to be the most possible generating mechanism of the blade-vortex interaction noise rather than a vortex-induced shock on the advancing side or a vortex-induced stall on the retreating side. Therefore, in the present prediction scheme the quadrupole source and the viscous stress contribution in the dipole source are both neglected from the acoustic source terms, leaving the blade thickness noise term and the blade-pressure-fluctuation term, both of which are sometimes called the linear source.

Then the sound field due to the blade-vortex interaction can be expressed as the following form:

$$4\pi p'(\vec{x},t) = \frac{\partial}{\partial t}\int\left[\frac{\rho_o v_n}{r\Lambda}\right]d\Sigma + \frac{1}{c}\frac{\partial}{\partial t}\int\left[\frac{p_b \cos\theta}{r\Lambda}\right]d\Sigma + \int\left[\frac{p_b \cos\theta}{r^2\Lambda}\right]d\Sigma \qquad (3\text{-}1)$$

where

$$\Lambda = (1 + M_n^2 - 2M_n \cos\theta)^{1/2} \qquad (3\text{-}2)$$

and standard notation is used. The first term in the right-hand side is due to a blade thickness effect, and the second term is due to a blade-pressure fluctuation effect on the far-field while the third term is on the near-field. A detailed description, which includes a numerical computation procedure, is given in the Appendix.

To predict the blade-vortex interaction noise, one must know the blade-surface-pressure distribution, P_b, during the interaction. In the present paper, measured instantaneous blade-pressure fluctuations during the selected flight condition are used to put into the dipole source term.

Measured Blade Pressure

Figures 4 and 5 are examples of measured pressure-fluctuation signal parametered by the spanwise station and by the chordwise station, respectively. Two distinct interactions are observed as a steep increasing slope of differential pressure on the advancing side. A rigid wake analysis suggests that the first one starting about 55° azimuth at the blade tip is an interaction with the 1-1/2-revolution old tip vortex, whereas the second one starting about 70° is the interaction with the 1-revolution old tip vortex. One additional interaction observed at the inboard stations cannot be explained by a rigid wake analysis; however, this phenomenon is quite repeatable through the following revolutions. It may have resulted from wake distortion due to mutual interactions of vortices, interaction with fuselage, or atmospheric turbulence. On the retreating side a big interaction with the 1-revolution old tip vortex is observed which starts from the blade root and ends up at about 290° at the tip. The azimuthal angle where the blade surface experiences the peak-pressure shifts with the span location. In other words, the blades interact with tip vortices at some oblique angle and the interaction point moves along the blade span with the blade rotation. Those pressure fluctuations due to interactions are strong around the leading edge portion and the outer radius, but not much interaction activity is seen beyond 20% of chord or within 60% of span.

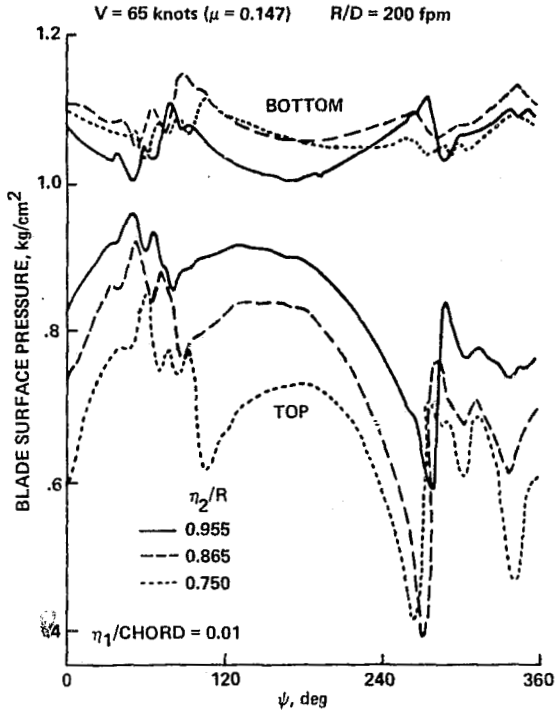


Figure 4. Example of blade surface pressure history at different span positions (Ref. 8).

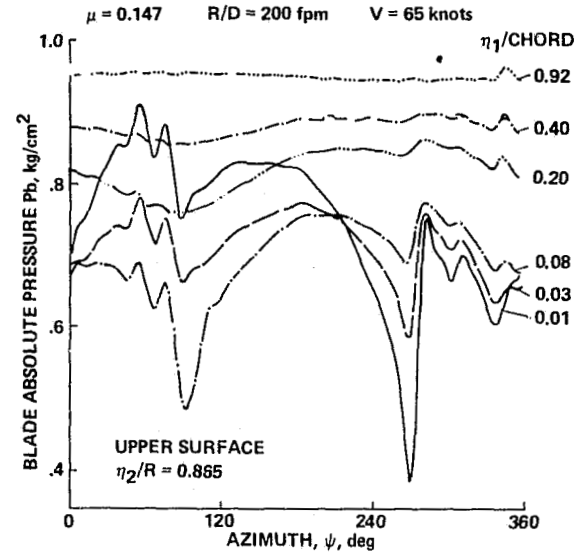


Figure 5. Example of blade surface pressure history at different chord positions (Ref. 8).

Modeling the Blade Pressure History

It may be instructive to describe original attempts to predict the interaction noise even though they have failed to give the interaction spike in the computed acoustic waveform. The first attempt was to put all measured surface-pressure data into the source term by specifying the mesh points of numerical calculation to be exactly the same point where the pressure sensors were located. The resulting acoustic waveform was just like the noise due to a steady loading because the mesh was too coarse to reflect the interaction effect.

Then the next step was to use an interpolation scheme along the rotor blade coordinate to provide a finer mesh; however, it did not improve the results. Figure 6 explains the reason for this. The strong solid lines are simple models of the blade-pressure fluctuation at several spanwise locations during an interaction with the tip vortices. The two broken lines, which were obtained by projecting the positive and the negative peaks of the blade-pressure fluctuation onto the rotor disk, indicate the direction of the blade-vortex interaction trajectory. The strong acoustic sources due to blade-vortex interaction are confined between these two broken lines. Because they have some skew angle to the polar radials, the interpolation along the blade-coordinate system cannot follow the pressure-fluctuation peaks at the intermediate span positions; consequently, the impulsive nature of the acoustic waveform may be smeared out. Therefore, the interpolation should be executed along interaction lines, which requires a lot of difficult work. First of all, it is very difficult for a computer to search for peak pressures and their positions from noisy data. Secondly, from these pressures and their positions along the interaction line, it is almost impossible to carry out an interpolation routine for each mesh point on the blade.

Instead of performing these laborious calculations of interpolation, measured surface-pressure histories are modeled in an analytical form as follows:

Since the surface pressure depends on the blade coordinates and azimuthal angle, the blade surface pressure, P_b, should be a function of these three variables.

$$p_b = p_b(\eta_1, \eta_2, \psi) \tag{3-3}$$

where η_1 is a chordwise coordinate, η_2 a spanwise coordinate, and ψ an azimuthal angle. After a model is described in simpler form and special attention given to the interaction trajectory, P_b can be written:

$$p_b = A_1(\eta_1)A_2(\eta_2)f\{\psi - \psi_i(\eta_2)\} \tag{3-4}$$

where $A_1(\eta_1)$ and $A_2(\eta_2)$ are the chordwise and the spanwise distribution functions, respectively, and the azimuthal distribution function $f(\psi)$ is defined to be a function of an angle from an interaction line $\psi_i(\eta_2)$. Figure 7 shows the measured results of azimuthal angles for positive and negative pressure peaks and the modeled interaction lines on the advancing side. It can be seen that blade-vortex interaction trajectories are well modeled by linear functions of spanwise position. The discrepancy in the inner radius is negligible because the source intensity becomes weak in this area. The interaction line model in Fig. 7 on $\psi - \eta_2$ plane can be mapped on the polar coordinate system as shown in Fig. 8. The shape of the azimuthal distribution function f is defined based on the measured blade surface-pressure history at 95.5% span and 1% chord where the source intensity becomes strong. As Fig. 9 shows, after obtaining a differential pressure history, low frequency components are eliminated to focus on the blade-vortex interaction effect, giving the azimuthal model function, $f(\psi)$. This is a general form of an azimuthal pressure distribution. The amplitude will be determined depending on the chordwise and spanwise distribution functions, $A_1(\eta_1)$ and $A_2(\eta_2)$ which are also obtained by averaging the fluctuating portion of measured data as shown in Figs. 10(a) and 10(b). The phase or the peak position will be given by the interaction lines which have been described previously.

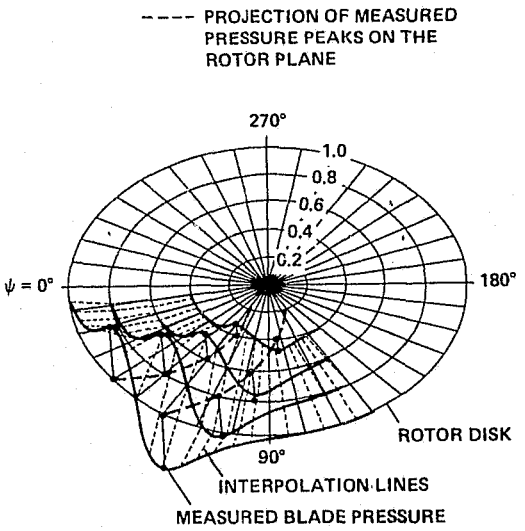


Figure 6. Interpolation of measured blade pressure.

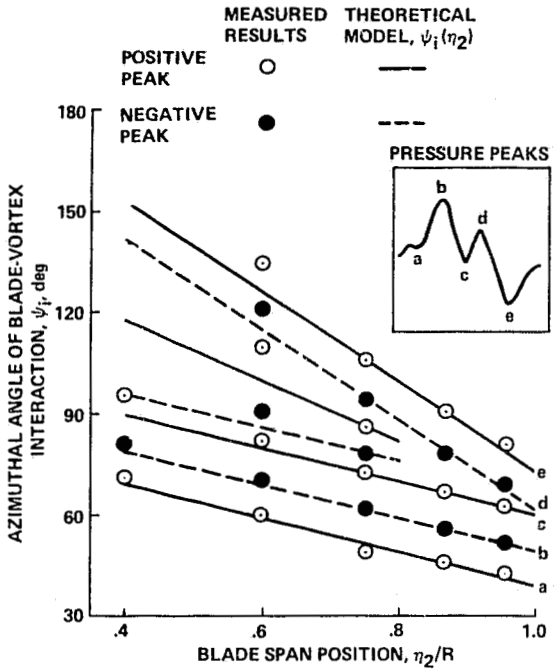


Figure 7. Modeling of blade-vortex interaction lines from measured results.

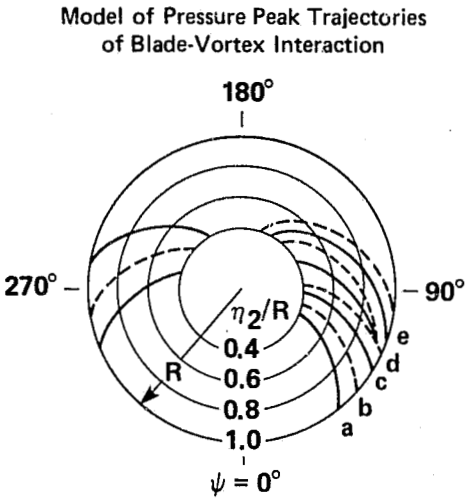


Figure 8. Blade-vortex interaction line model on rotor disk.

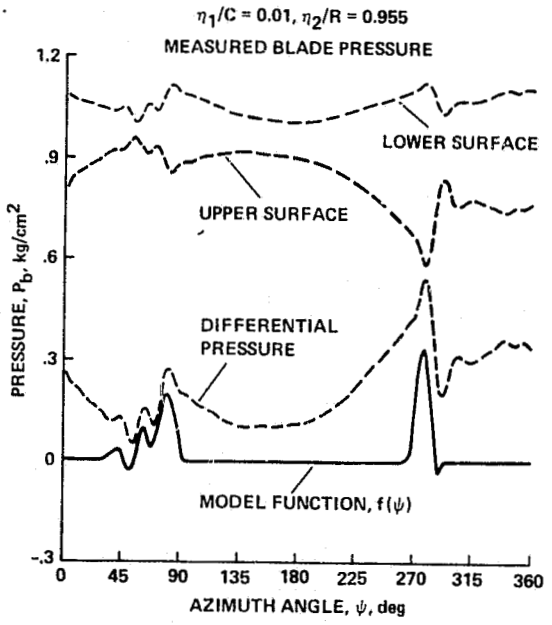


Figure 9. Modeling of azimuthal pressure distribution.

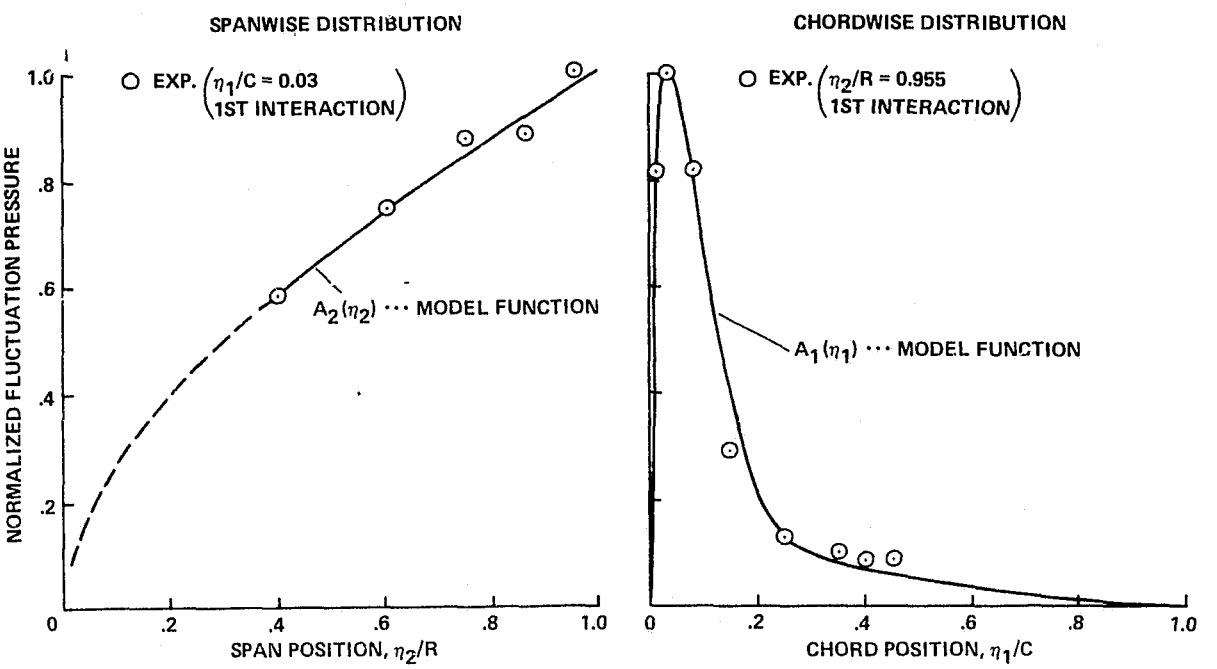


Figure 10. Modeling of spanwise and chordwise pressure distribution.

4. COMPARISON OF MEASURED AND COMPUTED ACOUSTIC WAVEFORM

Figures 11 and 12 show the comparison of the measured and computed acoustic waveforms for the right wing microphone and nose boom microphone, respectively. The general waveform, including the impulsive shape, is well predicted in both observer positions; however, the peak amplitudes are underestimated and the pulse widths overestimated. These discrepancies can be seen more clearly by expanding the pulse portion as in Fig. 13. Two possible reasons for these are: the differences in the frequency response characteristics of the data acquisition systems for the noise measurement and blade-pressure measurement (the noise measurement is 10 kHz and the blade-pressure measurement is 400 Hz). A response of 400 Hz can only catch the events of every 5° in azimuth, but the measured acoustic impulse shows about 1 msec of pulse width during which the blade may rotate about 2°. This low capability in blade-pressure frequency response would result in an underestimation in amplitude and a widening of the pulse width. The time differentiation to calculate the far-field noise that gives the interaction pulses in the acoustic waveform, may enhance these errors.

The second is the sparsity of measured pressure information along the blade span and also at the very leading edge. With only five pressure stations along the blade it is difficult to follow the interaction lines on the rotor disk plane. And because the significant pressure fluctuation due to the blade-vortex interaction can be observed only in the first few percent of the blade chord (where the blade surface slope changes drastically) it is necessary to make high resolution measurement at the leading edge.

One thing to be noted in Fig. 13 is that the expanded measured acoustic impluse has a very symmetric shape, indicating no significant transonic shock effect; in other words, the linear acoustic theory may be good enough for the prediction of this acoustic impluse.

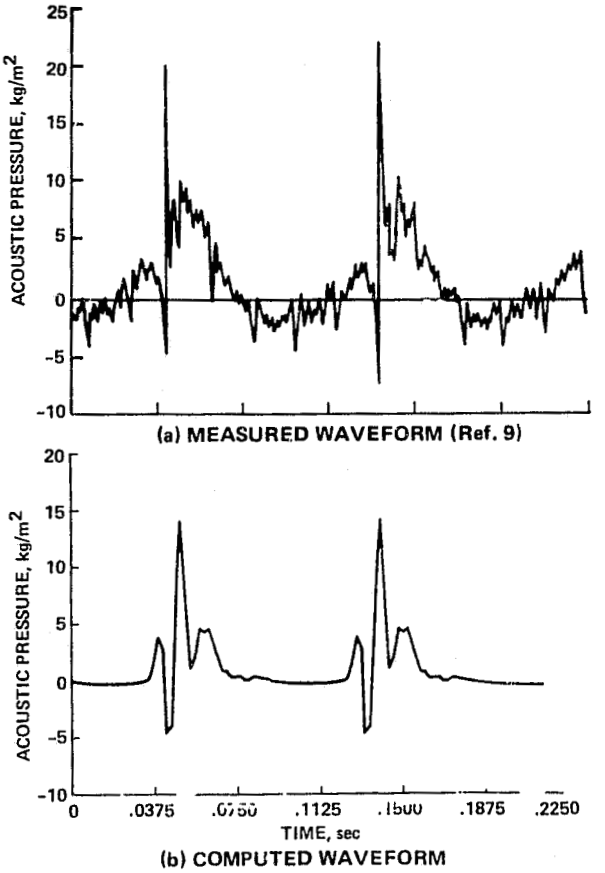


Figure 11. Comparison of acoustic waveform between measurement and computation (right wing microphone).

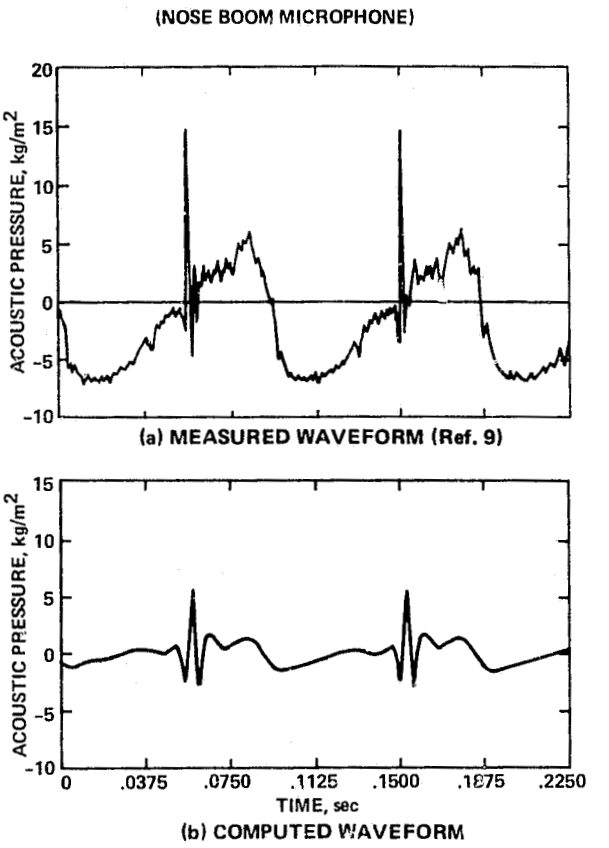


Figure 12. Comparison of acoustic waveform between measurement and computation (nose boom microphone).

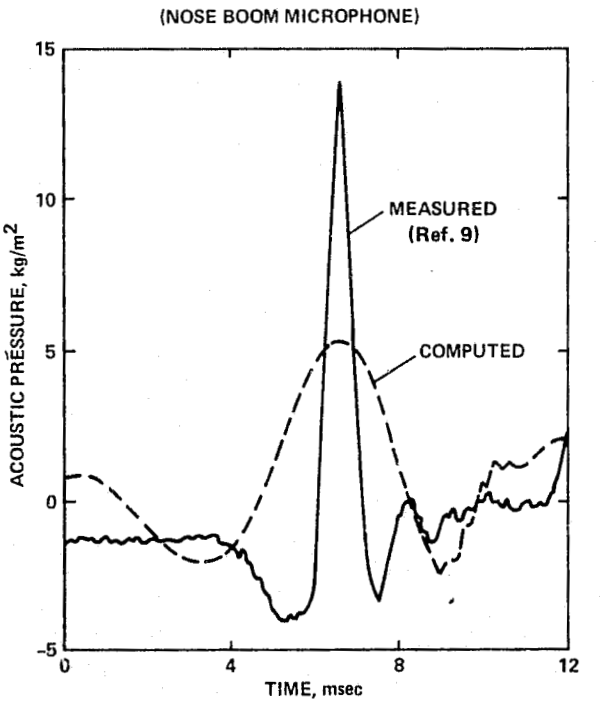


Figure 13. Comparison of expanded acoustic impulse between measurement and computation (nose boom microphone).

5. PHYSICAL EXPLANATION

Waveform of Blade-Vortex Interaction Noise

The general characteristics of the acoustic waveform due to blade-vortex interactions can be obtained by a simple two-dimensional physical model: a blade element encounters a vertical gust. When a blade is approaching a vortex whose velocity distribution is given as in Fig. 14(a), the blade experiences the change of angle of attack and then the differential pressure (Fig. 14(b)). The acoustic source intensity I changes in the same manner as the differential pressure for an observer located beneath the rotor plane (Fig. 14(c)).

The time derivative of the source intensity gives the far-field noise waveform. Figure 14(d) shows a typical positive spike of blade-vortex interaction noise radiating beneath the rotor.

This simple analysis suggests the following interesting facts: 1) The interaction acoustic impulse is generated at the instance that the vortex core hits the blade leading edge. 2) The pulse amplitude is proportional to the tangential velocity gradient in the core of the tip vortex, whereas the pulse width is proportional to the vortex-core diameter. 3) The sign of pulse depends on the rotational direction of tip vortex relative to the approaching blade and also on the observer position relative to the rotor disk.

Geometrical Relation Between the Interaction Trajectory and the Acoustic Planform

The geometrical relation between the blade-vortex interaction line and the acoustic planform is a dominating factor on the blade-vortex interaction noise. The broken line in Fig. 15 shows the measured blade-vortex interaction lines on the rotor disk, whereas the solid lines indicate the acoustic lines which are

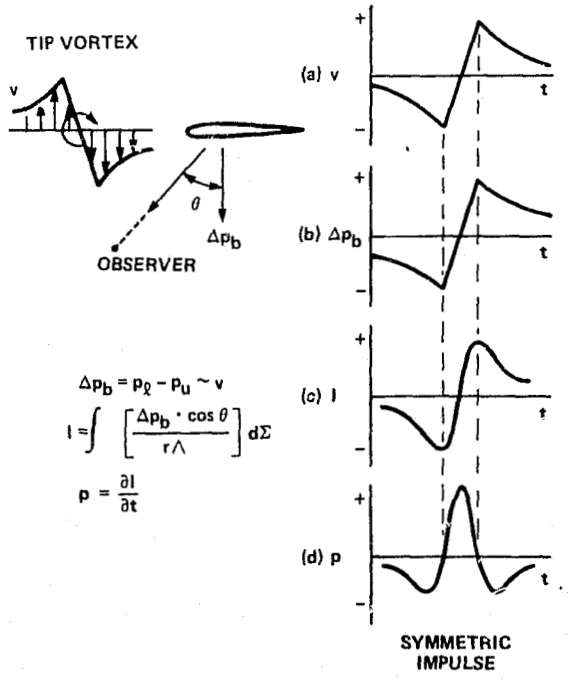


Figure 14. Formation of acoustic impulse due to blade-vortex interaction.

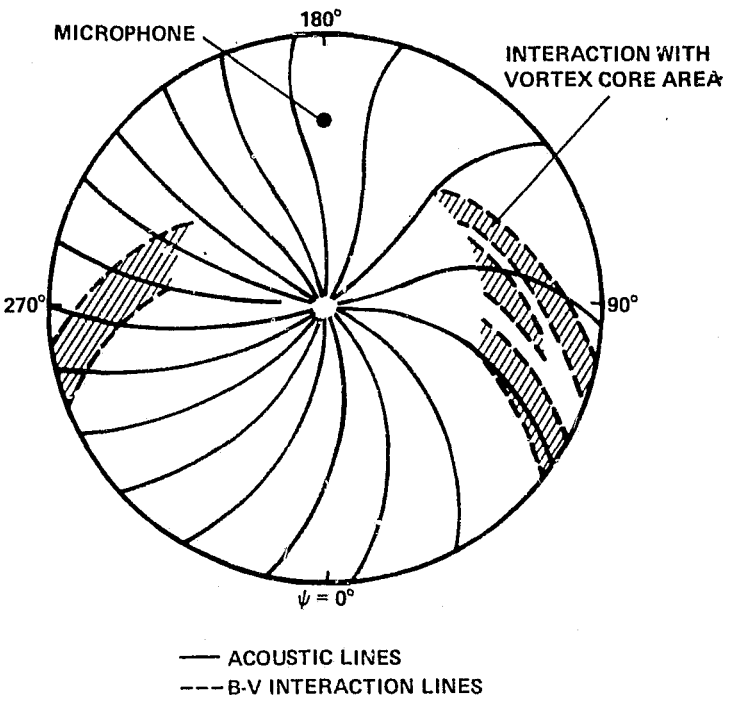


Figure 15. Coincidence between acoustic lines and blade-vortex interaction lines.

obtained by tracing interaction points of a blade leading edge and a contracting acoustic sphere at different but equally spaced observer times. The interaction lines are obtained by connecting the measured pressure-fluctuation peak positions during the blade-vortex interaction which are shown in Fig. 7. The hatched areas correspond to the interaction with the core region of the tip vortex where the velocity gradient is steepest and therefore the acoustic intensity becomes maximum.

To calculate blade-vortex interaction noise, it is necessary to integrate the acoustic sources distributed on the acoustic planform. When this interaction line becomes parallel to the acoustic line, the integration of acoustic sources may be performed "in-phase." This means that all the strong sources on the interaction line will accumulate together to radiate toward the observer and make a big acoustic interaction impulse.

On the other hand, when these lines make an oblique angle to the interaction line the acoustic sources may be integrated out of phase, i.e., they sometimes subtract from each other, thus reduce acoustic impulse at the observer position.

In Fig. 15, the interaction with the 1-1/2-revolution old tip vortex on the advancing side seems to be coinciding better with the acoustic lines than other interactions and causes the most effective in-phase radiation toward the microphone. The second interaction with the 1-revolution old tip vortex has less coincidence with the acoustic lines and generates a small spike. The measured acoustic waveform shows good coincidence with the above discussion on the source locations of the main impulse or the occasionally observed small impulse. The acoustic impulse due to interactions on the retreating side is hardly recognized in the measurement and calculation, even though the fluctuating pressure amplitude is larger than that on the advancing side. This is because, as Fig. 15 shows, the interaction lines do not coincide at all with acoustic lines specifically at the tip region where the stronger acoustic sources are distributed.

Trace Mach Number*

The concept of "trace Mach number" will be introduced here which helps to understand the blade-vortex interaction noise. This intersection point traces along the tip-vortex trajectory with the blade rotation, generating the interaction sound successively to every direction. The moving velocity of the intersection point is named the "trace Mach number M_{TR}" which is given by the following equation:

$$M_{TR} = R\Omega(x + \mu \sin \psi)/(c \sin \beta)$$

where β is the angle between the leading edge and the interaction line, and standard notation is used. As shown in Fig. 16 the interaction angle β changes

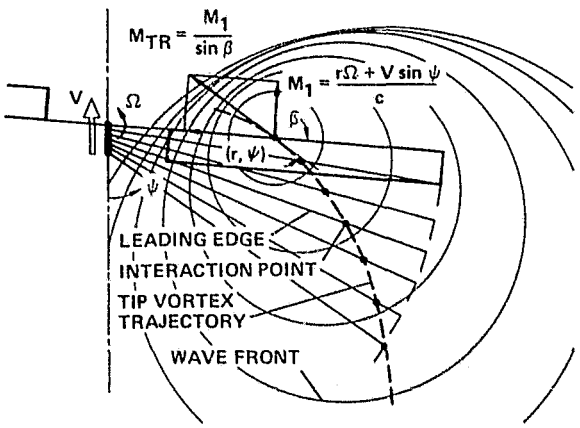


Figure 16. Trace Mach number M_{TR} of blade-vortex interaction and sound wave front.

when the blade rotates over a curved tip vortex trajectory, and M_{TR} could range from a local rotational Mach number M_1 to infinity with a decrease in the interaction angle. When M_{TR} is equal to or greater than unity, all the disturbances due to the interaction can be accumulated to make a vertical wave front or a Mach cone along the interaction line. Even if M_{TR} is less than unity the steep wave front could be generated somewhere because of the curved interaction line. It may appear as an overlap or an envelop of successive sound wave fronts. When the direction cosine of M_{TR} to the observer, which can be called as a "relative trace Mach number," is equal to unity a big sound impulse may be observed. The relative trace Mach number, $M_{TR,R}$, is then written as

*This concept was given by F. H. Schmitz initially. The similar idea was found in the literature [3] as "convection Mach number."

$$M_{TR,R} = M_{TR} \cos \gamma$$
$$= M_{TR} \vec{e} \cdot \vec{r}/r \qquad (5\text{-}1)$$

where γ is the angle between the unit tangential vector of the tip vortex $\vec{e}$ and the radiation direction vector $\vec{r}$.

6. CONCLUDING REMARKS

Impulsive noise caused by blade-vortex interaction was calculated by a linear noncompact acoustic theory using measured blade surface pressure fluctuations during low speed descending flight.

This result was compared with the simultaneously recorded noise signal. General agreement including the impulsive feature was obtained with the use of an analytical blade pressure distribution model made from the measured results. However, the expanded acoustic waveform showed an underestimation in pulse amplitude and an overestimation in pulse width. These discrepancies could be caused by the insufficient frequency response of the blade-pressure data-acquisition system and also insufficient blade pressure measurement locations to enable accurate plotting of the blade-vortex interaction pressure peak.

The vortex trajectory is extremely important for the interaction noise because its geometrical relation to the blade acoustic planform dominates the impulsive nature of sound. In fact, it was shown that the observed acoustic impulse was caused by the tip vortex (probably the 1-1/2 revolution old) parallel to the acoustic planform of the blade leading edge. In such condition, all the acoustic sources along the vortex trajectory are added together "in-phase" to produce a large acoustic impulse at the observer location. This mechanism was shown as an overlap or an envelope of wavefronts from the acoustic source moving at "the trace Mach number," which was defined as the speed of motion of the blade-vortex interaction point.

The basic shape of the impulsive acoustic waveform, such as sign, amplitude, and width of pulse, was also explained in relation to the vortex structure by a simple two-dimensional interaction model.

APPENDIX

Noncompact Linear Acoustic Theory

The analysis begins with the well-known Ffowcs Williams and Hawkings formulation (Ref. 10), in which the sound radiated by surfaces in motion is expressed as the integral equation:

$$4\pi p'(\vec{x},t) = \frac{\partial}{\partial t}\int\left[\frac{\rho_0 v_n}{r|1-M_r|}\right] dS - \frac{\partial}{\partial x_i}\int\left[\frac{P_{ij}n_j}{r|1-M_r|}\right] dS$$

$$+ \frac{\partial^2}{\partial x_i \partial x_j}\int\left[\frac{T_{ij}}{r|1-M_r|}\right] dV \qquad \text{(A1)}$$

where

$$T_{ij} = \rho v_i v_j + p_{ij} - c^2\rho'\delta_{ij}$$

and standard notation is assumed.

The right-hand side of the equation shows the respective contribution to the radiated sound field classified acoustically as monopole, dipole, and quadrupole noises. Physically speaking they are generated by the effects of the blade thickness, the viscous stress and pressure distribution on the blade, and the nonlinear flow fields such as turbulence or transonic perturbed flow with local shock waves around the blade, respectively. In the present calculation of blade-vortex interaction noise the last term and the viscous stress contribution in the second term are both neglected. Therefore, the blade thickness effect and the blade-surface-pressure fluctuation effect, both of which are often called the linear source, are left as the acoustic source terms in the right-hand side of equation (A1).

By replacing $P_{ij}n_j$ in the second term with $P_b \cos\theta$, where P_b is the blade surface pressure and θ is the angle between the radiation direction (observer direction) and outward normal to the blade surface, equation (A1) becomes:

$$4\pi p'(x,t) = \frac{\partial}{\partial t}\int\left[\frac{\rho_0 v_n}{r\Lambda}\right] d\Sigma + \frac{1}{c}\frac{\partial}{\partial t}\int\left[\frac{P_b \cos\theta}{r\Lambda}\right] d\Sigma + \int\left[\frac{P_b \cos\theta}{r^2\Lambda}\right] d\Sigma \qquad \text{(A2)}$$

in which the spatial differentiation is converted to a time differentiation and the integral coordinate system is changed using the following relation:

$$\frac{d\Sigma}{\Lambda} = \frac{dS}{|1-M_r|} \qquad \text{(A3)}$$

$$\Lambda = (1 + M_n^2 - 2M_n \cos\theta)^{1/2} \qquad \text{(A4)}$$

where S denotes a blade surface at a given time whereas Σ means a blade surface at a retarded time. In any case, the surface integration on the blades means the noncompact treatment of acoustic sources. The second term in equation (A2) is the blade-surface-pressure fluctuation contribution to the far-field radiation, whereas the third term is near field.

Computational Scheme Using Acoustic Planform

The actual computation was executed in the following manner. First, the source time τ is calculated for a specified observer time t and blade coordinates (η_1,η_2) to solve the retarded time equation with an iterative method. Then the azimuthal angle ψ at the retarded time will be computed. Now the blade surface pressure data can be quoted by the specified set of parameter (η_1,η_2,ψ) to

give an acoustic source intensity $p_b \cos \theta / r\Lambda$. These azimuthal angle calculations of the blade leading edge and the trailing edge provides the acoustic planforms of the rotating blades. These are the blade surfaces at a retarded time. Figure A1 shows the formation process of the acoustic planform surrounded by the solid lines. They are formed by the intersection surface of the rotating blades and the acoustic sphere contracting toward the observer at the speed of sound. A different observer time gives a different acoustic planform as shown by a broken line in Fig. A1. All the sound emitted from the same acoustic planform can be observed at the same time. After obtaining the source-intensity distribution over the blade surfaces at a retarded time, a numerical integration can be performed to get the resultant acoustic pressure for the given observer time and position. By repeating this procedure for successive observer times during one blade passing period, the acoustic time signal will be obtained. It can be said that the near-field noise is proportional to the above integrated values, whereas the far-field noise is given by its time derivatives. Figure A2 shows the flow chart of these procedures.

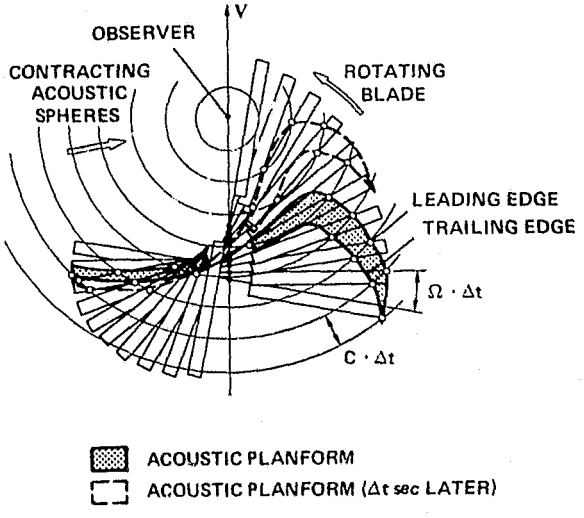


Figure A1. Formation of acoustic planform.

ACKNOWLEDGMENTS

The author would like to express his gratitude to the people in the Aeromechanics Laboratory for the grateful help, especially to Mr. Andy Morse, Dr. Fred Schmitz, Dr. Yung Yu, Mr. Don Boxwell, and Dr. Frank Caradonna for their creative discussions and valuable suggestions. He also acknowledges the support in data acquisition by the people of NASA Ames Research Center and Bell Helicopter Co. This study was made possible by the National Research Council Associateship.

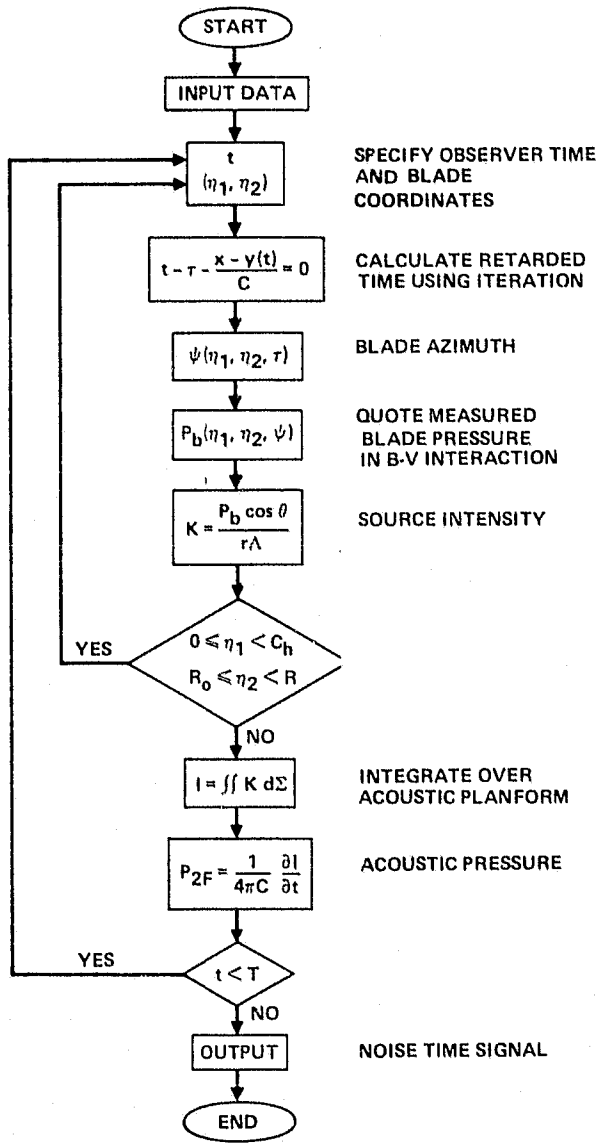


Figure A2. Prediction scheme of blade-vortex interaction noise.

REFERENCES

1. S. Widnall — Helicopter Noise Due to Blade-Vortex Interaction. J. Acoustical Soc. America, Vol. 50, No. 1 (part 2), 1971.

2. S. Widnall, T. L. Wolf — Effect of Tip Vortex Structure on Helicopter Noise Due to Blade-Vortex Interaction. J. Airc., Vol. 17, No. 10, Oct. 1980.

3. M. V. Lowson, J. B. Ollerhead — Studies of Helicopter Rotor Noise. USAAVLABS Tech. Rep. 68-60, Jan. 1969.

4. J. L. Tangler — Schlieren and Noise Studies of Rotors in Forward Flight. Presented at the 33rd Annual Forum of the American Helicopter Soc., Washington, D.C., May 1977.

5. D. R. Hoad — Helicopter Model Scale Results of Blade-Vortex Interaction Impulsive Noise as Affected by Tip Modification. Presented at the 36th Annual Forum of American Helicopter Soc., Washington, D.C., May 1980.

6. F. H. Schmitz, D. A. Boxwell — In-Flight Far Field Measurement of Helicopter Impulsive Noise. J. American Helicopter Soc., Vol. 21, No. 4, Oct. 1976.

7. D. A. Boxwell, F. H. Schmitz — Full-Scale Measurements of Blade-Vortex Interaction Noise. Presented at the 36th Annual Forum of the American Helicopter Soc., Washington, D.C., May 1980.

8. G. A. Shockey, T. W. Williamson, C. R. Cox — Helicopter Aerodynamics and Structural Loads Survey. Presented at the 32nd Annual Forum of the American Helicopter Soc., Washington, D.C., May 1976.

9. P. C. Sakowski, Jr., B. D. Charles — Noise Measurement Test Results for AH-1G Operational Loads Survey. Vols. I and II, Bell Helicopter Co. Rep. 299-099-831, Oct. 1976.

10. J. E. Ffowcs Williams, D. L. Hawkings — Sound Generation by Turbulence and Surfaces in Arbitrary Motion. Philosophical Transactions of the Royal Society of London, Series A, Vol. 264, May 8, 1969, pp. 321-342.